PAPER

Au-on-Ag nanostructure for *in-situ* SERS monitoring of catalytic reactions

View the article online for updates and enhancements.

Au-on-Ag nanostructure for *in-situ* SERS monitoring of catalytic reactions

Shuyue He[1] ⓘ**, Di Wu**[1]**, Siwei Chen**[2]**, Kai Liu**[1] ⓘ**, Eui-Hyeok Yang**[2] ⓘ**, Fei Tian**[1] **and Henry Du**[1,*]

[1] Department of Chemical Engineering and Materials Science, Stevens Institute of Technology, Hoboken, NJ 07030, United States of America
[2] Department of Mechanical Engineering, Stevens Institute of Technology, Hoboken, NJ 07030, United States of America

E-mail: hdu@stevens.edu

CrossMark

Abstract

Dual-functionality Au-on-Ag nanostructures (AOA) were fabricated on a silicon substrate by first immobilizing citrate-reduced Ag nanoparticles (Ag NPs, $\sim$43 nm in diameter), followed by depositing $\sim$7 nm Au nanofilms (Au NFs) via thermal evaporation. Au NFs were introduced for their catalytic activity in concave-convex nano-configuration. Ag NPs underneath were used for their significant enhancement factor (EF) in surface-enhanced Raman scattering (SERS)-based measurements of analytes of interest. Rhodamine 6G (R6G) was utilized as the Raman-probe to evaluate the SERS sensitivity of AOA. The SERS EF of AOA is $\sim$37 times than that of Au NPs. Using reduction of 4-nitrothiophenol (4-NTP) by sodium borohydride (NaBH$_4$) as a model reaction, we demonstrated the robust catalytic activity of AOA as well as its capacity to continuously monitor via SERS the disappearance of reactant 4-NTP, emergence and disappearance of intermediate 4,4$'$-DMAB, and the appearance of product 4-ATP throughout the reduction process in real-time and *in situ*.

Supplementary material for this article is available online

Keywords: Au-on-Ag nanostructure, thermal evaporation deposition, catalytic reaction, surface-enhanced Raman spectrum

(Some figures may appear in colour only in the online journal)

1. Introduction

Plasmonic metal nanostructures exhibit a multitude of fascinating and unique properties that have enabled their exploration for diverse applications such as catalysis [1–4], sensing [5–7], and photodynamic therapy [8]. The plasmonic responses depend strongly on the type, size, configuration, and surrounding environment of the metal nanostructures [9–12]. There is a growing interest in hybrid metal-metal nanostructures to take full advantage of the distinct properties of the constituent metal phases for their synergistic effect [13]. For example, bimetal core–shell or core-satellite structures can produce superior chemical and physical functionalities for the investigation of nanophotonics and catalysis [14–17].

Among many bimetal nanostructures, Ag–Au composites with different structural configurations have been proposed, especially for SERS-based sensing [18, 19], such as Ag/Au nanowires [20], Ag–Au alloy [9], Ag–Au cuboctahedra [21] and Ag–Au concave nanocrystal [22]. SERS utilizes the localized surface plasmon resonance (LSPR) of plasmonic nanostructures induced by laser irradiation to achieve multiple orders of magnitude enhancement of Raman scattering for detection and measurements of target analytes at concentrations as low as single molecules [23]. While the EF of Ag nanostructure is typically two orders of magnitude higher than its Au counterpart [24], its susceptibility to environmental degradation such as oxidation is the main drawback. In

---

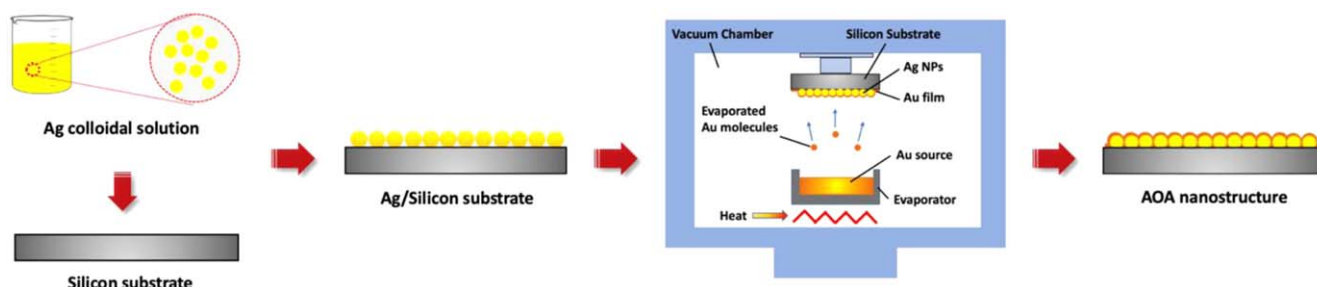* Author to whom any correspondence should be addressed.

Figure 1. Schematic of the steps in AOA nanostructure fabrication.

contrast, Au is well known for its chemical stability, biocompatibility and catalytic activity [16, 25, 26]. Ag core/Au shell nanostructures have thus been broadly investigated, including the use of such structures for SERS-based measurements of catalytic reactions.

One common approach to fabricate the Ag/Au core–shell nanostructure is to deposit Au atoms on Ag NPs through seeded growth via solution chemistry [27, 28]. Seeded growth has emerged as a common route to the synthesis of nanocrystals of many noble metals, such as Ag [29], Au [30], Pd [31] and Pt [32]. Though remarkably robust, the capability of seeded growth is restricted to metals that will not undergo galvanic replacement between them[16]. It is well documented that galvanic reaction occurs spontaneously and instantaneously when Ag NPs are mixed with $HAuCl_4$ in an aqueous solution [33–35]. It can be challenging to fabricate Ag/Au core/shell nanostructures free of pores due to galvanic replacement using the solution route [36].

Here, we report a facile method to produce the dense Au shell onto Ag NPs through thermal evaporation deposition (TED), which is not readily achievable via solution-based galvanic replacement reaction. The resultant AOA nanostructure is chemically stable and highly SERS- and catalytic-active by virtue of the 7 nm thin Au coating on Ag. Using Rhodamine 6G (R6G) as a model analyte, we demonstrated that the SERS EF of the AOA nanostructure is ~37 fold as large as that of Au NPs. Furthermore, the dual functionality of our AOA nanostructure, i.e., SERS activity of Ag NPs and the catalytic effect of the deposited Au, enabled sensitive *in situ* measurements of the reduction of 4-NTP by $NaBH_4$ to form 4-ATP in real-time.

2. Experiment section

2.1. Materials

Sodium borohydride ($NaBH_4$, 99%), ethanol (anhydrous, 99.8%), poly(allylamine hydrochloride) (PAH, Mw = 15000), sodium hydroxide (0.1 M NaOH standard solution, volumetric), 4-nitrothiophenol (4-NTP, 80%) and Rhodamine 6G (R6G) were purchased from Sigma-Aldrich. Sodium citrate trihydrate ($C_6H_5Na_3O_7 \cdot 3H_2O$) and hydrogen peroxide (H_2O_2, 30 wt% in water) were procured from Fisher Scientific. Silver nitrate (ultrapure, grade) was purchased from Across. Gold nanoparticles (Au NPs, 50 nm, in citrate solution) were

purchased from Nanocomposix. Milli-Q ultrapure water (no less than 18.2 MΩ) was used in the synthesis.

2.2. Synthesis of Ag NPs

Ag NPs were synthesized by a refined Lee and Meisel method [37] with the incorporation of UV irradiation. Details of which could be found elsewhere [38]. Briefly, 1 wt% aqueous sodium citrate (0.8 ml) was added to $AgNO_3$ solution (1 mM, 40 ml), drop by drop. The mixture was placed under a UV lamp (UV Flood Curing System, Cure Zone 2 (CONTROL-CURE, Chicago, IL)) for 4 h with gentle stirring.

2.3. Preparation of AOA nanostructure

Monodispersed Ag NPs were immobilized on a silicon substrate (with a native oxide layer), as shown in figure 1. The immobilization steps are as follows. The substrate was precoated by poly(allylamine hydrochloride) (PAH) polymer to minimize the agglomeration of metal nanoparticles. PAH was first dissolved in purified water filtered with Barnstead ion-exchange columns and further purified by passing through Millipore (Milli-Q) columns. The pH of the PAH aqueous solution was adjusted to 9, modified by sodium hydroxide (0.1 M NaOH standard solution). The substrate was exposed to the PAH aqueous solution for 30 min, then rinsed with Milli-Q water to remove any free or loosely bound PAH molecules [1]. Next, Ag NPs colloidal solutions were added dropwise 40 μl onto the PAH-covered silicon substrate, kept in the petri dish for 2 h and then rinsed with Milli-Q water to remove free and loosely bound Ag NPs. Substrates with immobilized Ag NPs were coated with 7 nm Au film from a heated Au source in a thermal evaporator (Angstrom Engineering, Ontario, Canada) [39, 40]. Briefly, the silicon substrate was held under high vacuum and exposed to gold vapor. The deposition speed was 0.03 nm s^{-1} with rotation speed of 30 rpm to ensure uniform deposition. The resultant AOA nanostructures supported on a silicon substrate were stored under sealed conditions filled with Argon gas before further use.

2.4. Sample preparation for in situ SERS monitoring of catalytic reactions

The AOA nanostructure supported on silicon substrate was immersed in 2 ml of 10 mM 4-NTP ethanol solution prefilled in a suspension culture plate. To facilitate the formation of a

self-assembled 4-NTP monolayer on the Au surface of AOA, the immersion was sealed and kept under inert gas ambient for 12 h. The AOA nanostructure with adsorbed 4-NTP was subsequently rinsed twice with Milli-Q water before the initiation of catalytic reaction while simultaneously being monitored by a Raman spectrometer. Au-catalyzed 4-NTP reduction was initiated by adding 100 μl of 5.28×10^{-2} M NaBH$_4$ solution on the AOA nanostructure with absorbed 4-NTP monolayer at room temperature. The time-resolved reaction process was monitored *in situ* by SERS.

2.5. Characterization

The Ag NPs and AOA nanostructures prepared were extensively characterized. Scanning electron microscope (SEM) images were obtained by ZEISS AURIGA at 5 kV with a working distance of 7.5 mm. SEM image analysis was performed using ImageJ software from the National Institutes of Health. Atomic force microscopy (AFM) was conducted with MultiView 2000^{TM}. Transmission electron microscope (TEM) images were obtained by FEI Titan Themis 200 at an acceleration voltage of 200 kV [41]. UV–visible absorption spectra were collected by a UV–vis spectrometer (synergy HT multidetection microplate reader, BioTek Instruments, Inc., Winooski, VT) [8].

Raman measurements were performed using a custom-built setup [1]. A 632.8 nm laser beam was spatially filtered and reflected from a Chroma 540DCLP dichroic mirror and excited the back aperture of a Thorlabs 20 $\times$ 0.55 N.A. objective. The excitation laser intensity in front of the objective was $\sim$8 mW. The well-sealed sample cell was placed on a Newport ULTRAlign 561D translation stage on an RS 3000 sealed hole tabletop with tuned damping to prevent undesirable oscillations. The Raman signal from the objective passed through the dichroic mirror. A collimator was used to focus the signal into a spectroscopic grade multimode fiber (400 μm core, Newport). A fiber-coupled Acton SpectraPro 2300 spectrometer with a Roper Scientific liquid nitrogen cooled CCD detector was used in spectral acquisition at a resolution of 2 cm^{-1}. All Raman measurements were performed using an acquisition time of 20 s (exposure time of 2 s $\times$ 10 integral exposures). A silicon wafer was used under 632.8 nm wavelength laser to calibrate the system before the measurement. After chemical reagents were introduced into the sample cell, the laser focus was adjusted to be on the AOA surface where reduction reaction takes place. Raman spectra were used as collected with background subtraction. All measurements were repeated three times.

3. Results and discussion

3.1. Structural characterization

As described in the previous experimental section, Ag NPs were prepared by wet chemical synthesis and Au coatings were deposited by TED. Figure 2(a) shows the SEM image of

Ag NPs as synthesized; the diameter of Ag NPs is 43 $\pm$ 6 nm. The surface coverage density of Ag NPs is 163 $\pm$ 16 particles μm^{-2} on a silicon substrate. Figure S1(a) (available online at stacks.iop.org/NANO/33/155701/mmedia) shows the TEM image of Ag NPs. The SEM image of Au film is shown in figure 2(b). The dark region to the left represents the surface of a bare substrate, created by parts of the Au film with a tweezer prior to measuring its thickness by AFM; the right bright region is the Au film. Figure S1(b) shows the TEM image of Au film; dark regions represent the Au island, which is also observed in the right side of figure 2(b). Figure 2(c) is a 2D-AFM image of the scratched Au film. The line scanning profiling over the 2D-AFM image suggests a Au film 7 nm thick (figure 2(d)). A 3D-AFM image further reviews the surface topography of Au film, shown in figure 2(e).

SEM and TEM images of AOA nanostructure are shown in figure 3(a) and S1(c)–(d), respectively. Figure S1(d) is a zoom in image of figure S1(c), demonstrated the Ag/Au core/shell nanostructure. The diameter of AOA structure is 52.04 $\pm$ 8.64 nm. SEM-energy dispersive X-ray (SEM-EDX) elemental mappings of Ag (blue), Au (yellow) and Ag/Au composition are shown in figures 3(b)–(d) respectively. EDX analysis provides the constituent Ag and Au elements in AOA (figure 3(e)). Besides, the UV–vis absorption spectra (figure S2) also demonstrated the characteristics of AOA and Ag NP nanostructures on Si substrate or in colloidal solution (in the case of Ag NPs).

To demonstrate the chemical stability of AOA nanostructures, we submerged both AOA on silicon and Ag NPs immobilized on silicon in 30 wt% H$_2$O$_2$ solutions for 30 min. Figure 4(a) shows the SEM image of Ag NPs after the H$_2$O$_2$ treatment. The inset is the image of the initial Ag NPs. Ag NPs have been completely dissolved in H$_2$O$_2$, consistent with documented studies [42]. Figure 4(b) depicts the SEM image of AOA after the same H$_2$O$_2$ treatment. The inset is the SEM image of the initial AOA. There is no apparent change in the structure of AOA and the coverage density of the underlying Ag NPs before and after the treatment, solid evidence of the chemical inertness of the Au thin film. The fact that Ag NPs were well-preserved is a strong indication of the dense quality of the Au coating by TED.

3.2. SERS measurement

To characterize the SERS activity of AOA nanostructures, we used R6G as a model analyte. Shown in figure 5 are Raman spectra of 10^{-6} M R6G obtained using an as-received silicon substrate, as-received Au NPs and AOA nanostructure (both of which are on silicon support). R6G typically exhibits vibrational modes at 1185 cm^{-1}, 1315 cm^{-1}, 1363 cm^{-1} and 1512 cm^{-1}, which can be assigned to the aromatic C–C stretching vibrations of R6G molecules [43]. No apparent R6G peaks were detected except at 520 cm^{-1} and 940 cm^{-1} associated with silicon, indicating the inability of regular Raman spectroscopy to detect 10^{-6} M R6G in the absence of plasmonic nanostructure. In contrast, Au NPs immobilized on silicon substrate yielded appreciable R6G Raman peaks (blue
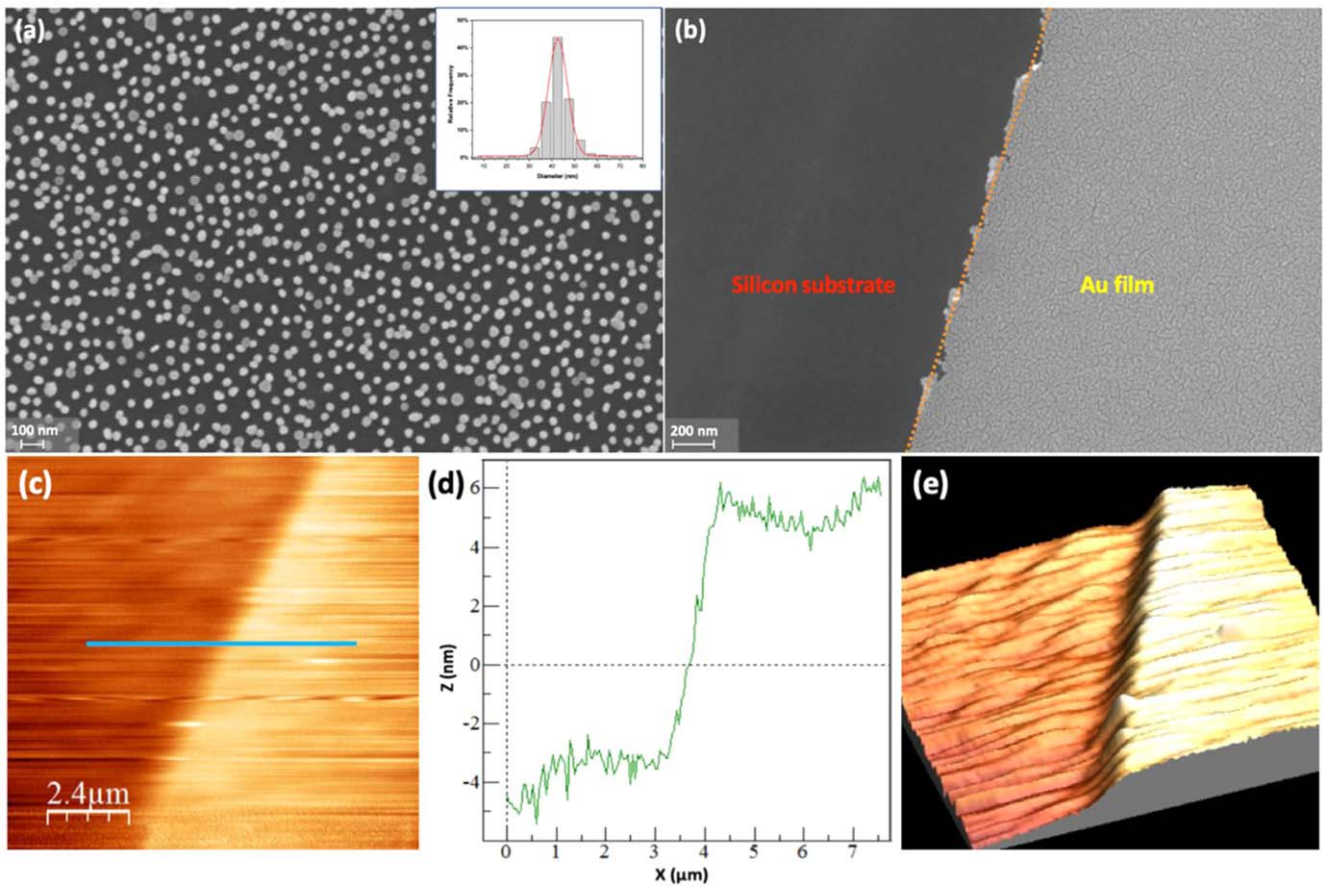
Figure 2. The SEM image of (a) Ag NPs (the inset is a statistical histogram of the diameter distribution of Ag NPs on a silicon substrate) and (b) Au film. (c) 2D-AFM image of Au film. (d) Line scanning profiling of 2D-AFM of Au film. (e) 3D-AFM image of Au film.
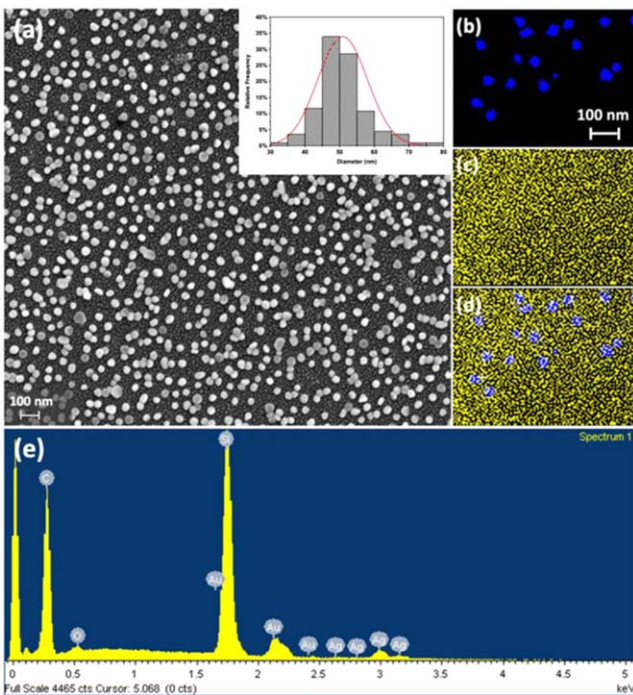

Figure 3. (a) The SEM image of AOA nanostructure. SEM-energy dispersive X-ray (SEM-EDX) elemental mapping of (b) Ag NPs, (c) Au film and (d) AOA. (e) EDX analysis of AOA.

line) at 1185 cm^{-1}, 1315 cm^{-1}, 1363 cm^{-1} and 1512 cm^{-1} due to the SERS activity of Au NPs. However, AOA produced the most striking signal enhancement with high intensities at the peaks characteristics of R6G, a clear sign of its robust SERS activity.

To evaluate the respective EFs of the Au NPs and AOA nanostructure, the intensities are normalized for the laser power with the collection conditions—acquisition time and detector sensitivity—remaining the same. We used the normalized 520 cm^{-1} Si peak as an internal standard for the subsequent EF calculations. The EFs were calculated for R6G molecules using the 1363 cm^{-1} peak according to the equation below [44]:

$$EF = \frac{I_{SERS}/C_{SERS}}{I_{NR}/C_{NR}}, \qquad (1)$$

where I_{SERS} and C_{SERS} are the Raman intensity and the concentration of R6G solution used in SERS measurement; I_{NR} and C_{NR} are the Raman intensity and the concentration of R6G solution used in routine Raman measurements. This analytical method provides a simple approach to comparing the SERS effect of different substrates without making specific assumptions of the surface densities of SERS-active sites and the surface density of adsorbed molecules [45]. The calculated EFs are 579, 2,1392 and 106,839, respectively, for Au NPs and AOA as well as Ag NPs (the SERS spectra are
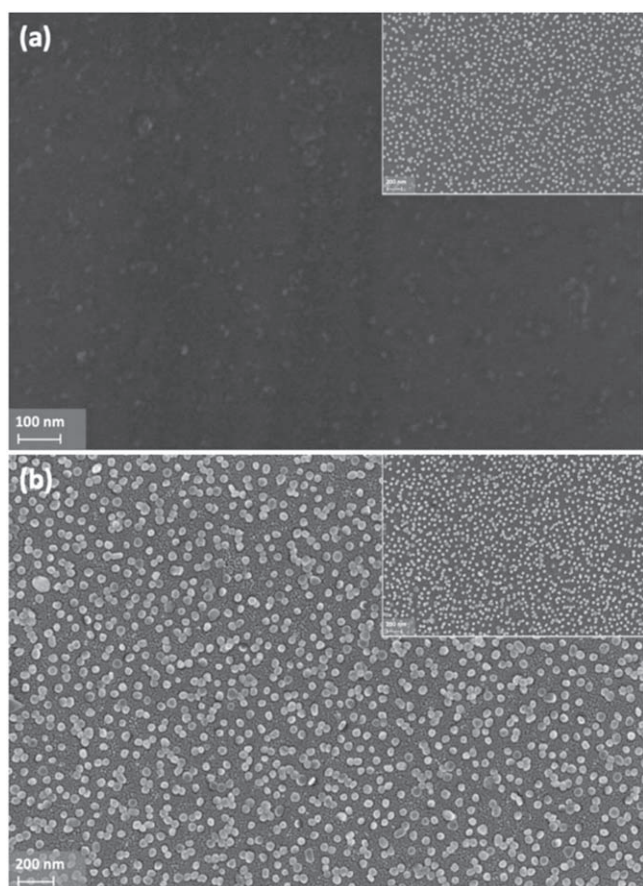
Figure 4. SEM image of Ag NPs after immersion in H_2O_2 solution for 30 min. The inset is an SEM image of as-prepared Ag NPs. (b) SEM image of AOA after identical H_2O_2 treatment. The inset is an SEM image of as-prepared AOA.
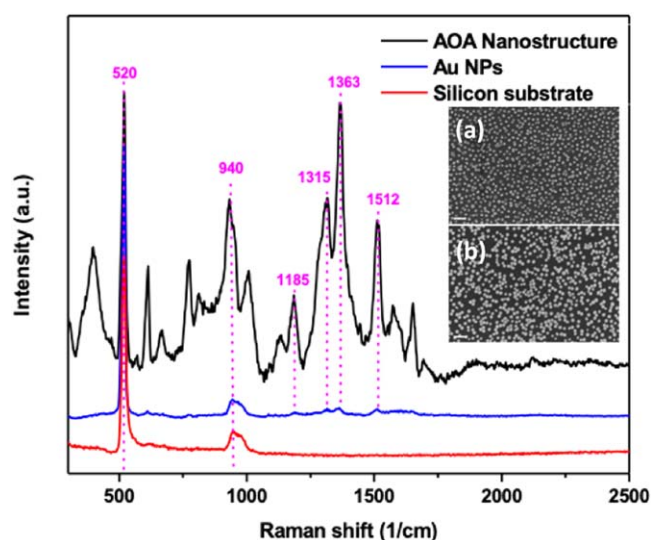

Figure 5. SERS spectra of 10^{-6} M R6G using an as-received silicon substrate, Au NPs and AOA. Inset (a) is the SEM image of AOA and inset (b) is the SEM image of Au NPs, scale bar is 200 nm. Each measurement was repeated three times.
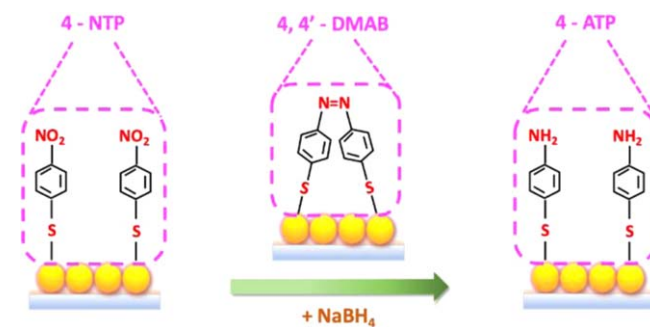

Figure 6. Schematic of a tentative mechanism of the Au-catalyzed reduction from surface-adsorbed 4-NTP by $NaBH_4$ to 4,4′-DMAB, and thus to 4-ATP.

shown in figure S3). Although the EF of AOA is not as high as that of Ag NPs, which is not surprising, the 37-fold increase over Au NPs in EF makes AOA a far more promising platform for sensitive SERS measurements while taking advantage of the catalytic effort of Au. As shown in table S1, our AOA nanostructure has SERS activity comparable to other Ag/Au composites.

3.3. In-situ SERS monitoring of catalytic reactions

The SERS activity of AOA allows for synergistic SERS-based monitoring of catalytic reactions should the Au thin film exhibit catalytic property. To demonstrate the potential of AOA in this regard, we chose as a model system the reduction of aromatic nitro compounds ($R-NO_2$) to aniline derivative ($R-NH_2$) by $NaBH_4$ in the presence of Au catalyst at room temperature, as shown in figure 6, given their significance for the environment and the synthesis of fine chemicals [9, 20–22].

AOA nanostructures with pre-adsorbed 4-NTP layer prepared as previously described were used for catalytic investigation. There are two possible pathways for 4-NTP reduction [46, 47], shown in figure S4. In this study, the 4-NTP layer underwent a two-step (red pathway), Au-catalyzed reduction process upon the introduction of $NaBH_4$ at room temperature. $NaBH_4$ reacts with water on the surface of nanocatalyst (AOA) and thus to produce hydrogen and an oxidized form of borohydride. The 4-NTP molecule gets reduced subsequently by the adsorbed oxidized $NaBH_4$ species to 4,4′-dimercapto-azobenzene (4,4′-DMAB). Due to the chemical instability of 4,4′-DMAB, it will continue to react until it is exhausted [48]. The final product was 4-ATP. As shown in figure 7, the SERS spectra of 4-NTP exhibited four characteristic vibrational bands at 856 cm^{-1}, 1112 cm^{-1}, 1347 cm^{-1} and 1571 cm^{-1}, corresponding to C–H wagging, C–S stretching, O–N–O stretching, and phenyl ring modes, respectively [45]. The SERS signal of 4-NTP remained unchanged in the first minute or so of the initiation of the reduction reaction. It is possible that active hydrogen species are formed at this time upon adsorption of borohydride ions
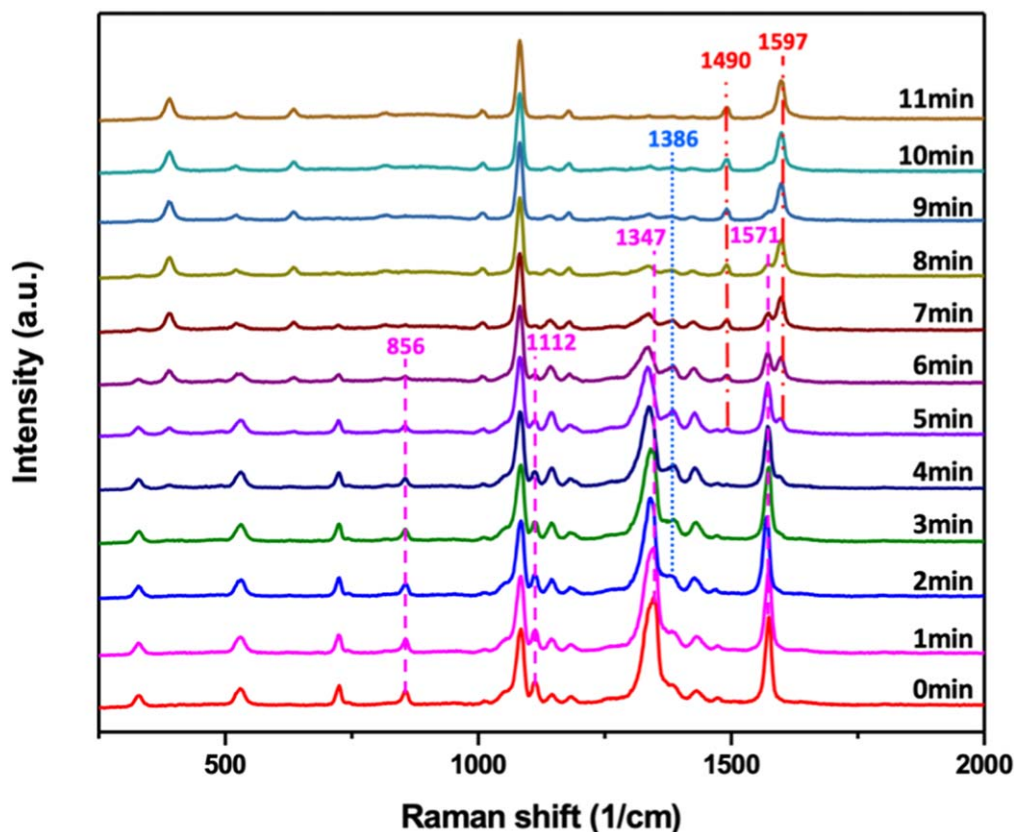
Figure 7. Time-resolved SERS spectra during Au-catalyzed reduction of 4-NTP to 4-ATP by NaBH$_4$ using AOA nanostructure on silicon substrate. The monitoring was repeated three times.

onto the surface of Au [49]. Hence, the hydrogenation of 4-NTP was initiated once the concentration of surface hydrogen species reached a threshold. As the reaction proceeded, the peaks of 4-NTP (856 cm^{-1}, 1112 cm^{-1}, 1347 cm^{-1} and 1517 cm^{-1}) decreased gradually, associated with steady depletion of $-$NO$_2$ groups. Concurrently, a vibrational band of some intermediate species emerged along the reaction pathway at 1386 cm^{-1}, which can be attributed to N=N stretching in 4,4′-DMAB. As reaction time increased, the intensity of SERS signals of 4,4′-DMAB intermediate first increased (from 2 min to 5 min), then decreased (from 5 min to 10 min), and finally disappeared thereafter as shown in figure 7. Accompanied with the diminishing intensity of the vibrational bands of 4-NTP and 4,4′-DMAB are the increasing peak intensity at 1597 cm^{-1} and the emergence of an additional band at 1490 cm^{-1}. These two bands correspond to phenyl ring mode [50] and aniline derivate (R-NH$_2$) [51], respectively, from 4-ATP, indicating the formation of 4-ATP as a reduction product. The time-resolved tracking of the disappearance of 4-NTP, emergence and disappearance of 4,4′-DMAB, and appearance of 4-ATP shown in figure 7 demonstrates the usefulness of the AOA for *in situ* monitoring of catalytic chemical reactions. As shown in figure S5, three sets of experimental results of SERS measurements for the chemical reaction demonstrated the replicability. Table S2 provides a summary of reported catalytic reaction regarding 4-NTP to 4-ATP by NaBH$_4$ through the two-step pathway on Ag/Au based platforms.

4. Conclusion

We used a facile method to fabricate AOA nanostructures on a silicon substrate. The TED technique employed to deposit thin Au film on Ag NPs overcomes the challenges associated with solution-based bimetal nanostructure synthesis due to galvanic replacement reactions. AOA is chemically stable in highly oxidative H$_2$O$_2$ solutions. It exhibits SERS EF that is $\sim$37 times higher than that of Au NPs. The concave-convex topography of Au thin film on immobilized Ag NPs possesses significant catalytic activity. The dual functionality of the AOA, i.e., SERS and catalytic activities, has enabled SERS-based monitoring of the catalytic reduction process of 4-NTP to 4-ATP by NaBH$_4$ in real-time and *in situ*. This investigation demonstrates that highly functional nanostructures can be fabricated using an easy-to-implement and scalable method. The unique properties of such nanostructures can be utilized synergistically to study the kinetics and mechanisms of catalytic reactions, including reaction pathways.

Data availability statement

All data that support the findings of this study are included within the article (and any supplementary files).

Author contributions

Shuyue He: Conceptualization, Methodology, Software, Validation, Formal analysis, Investigation, Data curation, Writing - original draft, Writing - review & editing, Visualization, Supervision. Di Wu: Methodology, Investigation, Writing - review & editing. Siwei Chen: Methodology, Software, Writing - review & editing. Kai Liu: Methodology, Resources. Eui-Hyeok Yang: Writing - review & editing, Resources. Fei Tian: Funding acquisition. Henry Du: Formal analysis, Conceptualization, Writing - review & editing, Resources, Supervision, Project administration, Funding acquisition.

Notes

The authors declare that they have no known competing financial interests or personal relationships that could have influenced the work reported in this paper.

ORCID iDs

Shuyue He ⓘ https://orcid.org/0000-0002-5770-7483
Kai Liu ⓘ https://orcid.org/0000-0003-3266-7427
Eui-Hyeok Yang ⓘ https://orcid.org/0000-0003-4893-1691

References

[1] Liu K, Chen T, He S, Robbins J P, Podkolzin S G and Tian F 2017 Observation and identification of an atomic oxygen structure on catalytic gold nanoparticles *Angew. Chem.—Int. Ed.* **56** 12952–7

[2] Scoullos E V, Hofman M S, Zheng Y, Potapenko D V, Tang Z, Podkolzin S G and Koel B E 2018 Guaiacol adsorption and decomposition on platinum *J. Phys. Chem. C* **122** 29180–9

[3] Liu K, He S, Li L, Liu Y, Huang Z, Liu T, Wu H, Jiang X, Liu K and Tian F 2021 Spectroscopically clean Au nanoparticles for catalytic decomposition of hydrogen peroxide *Sci. Rep.* **11** 9709

[4] Tang Z, Chen T, Liu K, Du H and Podkolzin S G 2021 Atomic, molecular and hybrid oxygen structures on silver *Langmuir* **37** 11603–10

[5] Pinkhasova P, Chen H, (Tiny) Verhoeven M W G M, Sukhishvili S and Du H 2013 Thermally annealed Ag nanoparticles on anodized aluminium oxide for SERS sensing *RSC Adv.* **3** 17954

[6] Liu K, Wuenschell J, Bera S, Tang R, Ohodnicki P R and Du H 2019 Nanostructured sapphire optical fiber embedded with Au nanorods for high-temperature plasmonics in harsh environments *Opt. Express* **27** 38125

[7] Liu K, Ohodnicki P R, Kong X, Lee S S and Du H 2019 Plasmonic Au nanorods stabilized within anodic aluminum oxide pore channels against high-temperature treatment *Nanotechnology* **30** 405704

[8] Hu Y, Yang Y, Wang H and Du H 2015 Synergistic integration of layer-by-layer assembly of photosensitizer and gold nanorings for enhanced photodynamic therapy in the near infrared *ACS Nano.* **9** 8744–54

[9] Han Q, Zhang C, Gao W, Han Z, Liu T, Li C, Wang Z, He E and Zheng H 2016 Ag–Au alloy nanoparticles: Synthesis and *in situ* monitoring SERS of plasmonic catalysis *Sensors Actuators* B **231** 609–14

[10] Dong J, Qu S, Zheng H, Zhang Z, Li J, Huo Y and Li G 2014 Simultaneous SEF and SERRS from silver fractal-like nanostructure *Sensors Actuators* B **191** 595–9

[11] Vassalini I, Rotunno E, Lazzarini L and Alessandri I 2015 Stainless' gold nanorods: preserving shape, optical properties, and sers activity in oxidative environment *ACS Appl. Mater. Interfaces* **7** 18794–802

[12] Li J N, Liu T Z, Zheng H R, Gao F, Dong J, Zhang Z L and Zhang Z Y 2013 Plasmon resonances and strong electric field enhancements in side-by-side tangent nanospheroid homodimers *Opt. Express* **21** 17176

[13] Ye X, Chen J, Diroll B T and Murray C B 2013 Tunable plasmonic coupling in self-assembled binary nanocrystal superlattices studied by correlated optical microspectrophotometry and electron microscopy *Nano Lett.* **13** 1291–7

[14] Ayala-Orozco C, Liu J G, Knight M W, Wang Y, Day J K, Nordlander P and Halas N J 2014 Fluorescence enhancement of molecules inside a gold nanomatryoshka *Nano Lett.* **14** 2926–33

[15] Li P, Ma B, Yang L and Liu J 2015 Hybrid single nanoreactor for *in situ* SERS monitoring or plasmon-driven and small Au nanoparticles catalyzed reactions *Chem. Commun.* **51** 11394–7

[16] Yang Y, Liu J, Fu Z W and Qin D 2014 Galvanic replacement-free deposition of au on ag for core–shell nanocubes with enhanced chemical stability and SERS activity *J. Am. Chem. Soc.* **136** 8153–6

[17] Zheng Y, Tang Z and Podkolzin S G 2020 Catalytic platinum nanoparticles decorated with subnanometer molybdenum clusters for biomass processing *Chem.—A Eur. J.* **26** 5174–9

[18] Xiong Y, Washio I, Chen J, Cai H, Li Z-Y and Xia Y 2006 Poly(vinyl pyrrolidone): A dual functional reductant and stabilizer for the facile synthesis of noble metal nanoplates in aqueous solutions *Langmuir* **22** 8563–70

[19] Toshima N and Wang Y 1993 Novel preparation, characterization and catalytic properties of polymer-protected Cu/Pd bimetallic colloid *Chem. Lett.* **22** 1611–4

[20] Zhu Y, Tang H, Wang H and Li J 2021 *In Situ* SERS monitoring of the plasmon-driven catalytic reaction by using single Ag@Au nanowires as substrates *Anal. Chem.* **93** 11736–44

[21] Zhang J, Winget S A, Wu Y, Su D, Sun X, Xie Z-X and Qin D 2016 Ag@Au concave cuboctahedra: a unique probe for monitoring au-catalyzed reduction and oxidation reactions by surface-enhanced raman spectroscopy *ACS Nano* **10** 2607–16

[22] Ahn J, Wang D, Ding Y, Zhang J and Qin D 2018 Site-selective carving and co-deposition: transformation of Ag nanocubes into concave nanocrystals encased by Au–Ag alloy frames *ACS Nano* **12** 298–307

[23] Kang L, Xu P, Zhang B, Tsai H, Han X and Wang H L 2013 Laser wavelength- and power-dependent plasmon-driven chemical reactions monitored using single particle surface enhanced Raman spectroscopy *Chem. Commun.* **49** 3389–91

[24] Jakab A, Rosman C, Khalavka Y, Becker J, Trügler A, Hohenester U and Sönnichsen C 2011 Highly sensitive plasmonic silver nanorods *ACS Nano* **5** 6880–5

[25] Cobley C M, Chen J, Cho E C, Wang L V and Xia Y 2011 Gold nanostructures: A class of multifunctional materials for biomedical applications *Chem. Soc. Rev.* **40** 44–56

[26] Barton D G and Podkolzin S G 2005 Kinetic study of a direct water synthesis over silica-supported gold nanoparticles† *J. Phys. Chem.* B **109** 2262–74

[27] Jana N R, Gearheart L and Murphy C J 2001 Wet chemical synthesis of high aspect ratio cylindrical gold nanorods *J. Phys. Chem.* B **105** 4065–7

[28] Sun Y, Gates B, Mayers B and Xia Y 2002 Crystalline silver nanowires by soft solution processing *Nano Lett.* **2** 165–8

[29] Pietrobon B, McEachran M and Kitaev V 2009 Synthesis of size-controlled faceted pentagonal silver nanorods with tunable plasmonic properties and self-assembly of these nanorods *ACS Nano* **3** 21–6

[30] Sau T K and Murphy C J 2004 Room temperature, high-yield synthesis of multiple shapes of gold nanoparticles in aqueous solution *J. Am. Chem. Soc.* **126** 8648–9

[31] Wang F, Li C, Sun L-D, Xu C-H, Wang J, Yu J C and Yan C-H 2012 Porous single-crystalline palladium nanoparticles with high catalytic activities *Angew. Chem.* **124** 4956–60

[32] Mahmoud, Tabor C E, El-Sayed M A, Ding Y and Wang Z L 2008 A new catalytically active colloidal platinum nanocatalyst: the multiarmed nanostar single crystal *J. Am. Chem. Soc.* **130** 4590–1

[33] Sun Y, Mayers B and Xia Y 2003 Metal nanostructures with hollow interiors *Adv. Mater.* **15** 641–6

[34] McEachran M, Keogh D, Pietrobon B, Cathcart N, Gourevich I, Coombs N and Kitaev V 2011 Ultrathin gold nanoframes through surfactant-free templating of faceted pentagonal silver nanoparticles *J. Am. Chem. Soc.* **133** 8066–9

[35] Hong X, Wang D, Cai S, Rong H and Li Y 2012 Single-crystalline octahedral Au–Ag nanoframes *J. Am. Chem. Soc.* **134** 18165–8

[36] Pinkhasova P, Puccio B, Chou T, Sukhishvili S and Du H 2012 Noble metal nanostructure both as a SERS nanotag and an analyte probe *Chem. Commun.* **48** 9750

[37] Lee P C and Meisel D 1982 Adsorption and surface-enhanced Raman of dyes on silver and gold sols *J. Phys. Chem.* **86** 3391–5

[38] Pinkhasova P, Yang L, Zhang Y, Sukhishvili S and Du H 2012 Differential SERS activity of gold and silver nanostructures enabled by adsorbed poly(vinylpyrrolidone) *Langmuir* **28** 2529–35

[39] Bai X *et al* 2017 Orientation control of solution-processed organic semiconductor crystals to improve out-of-plane charge mobility *Chem. Mater.* **29** 7571–8

[40] Zhang Y, Chen A, Kim M W, Alaei A and Lee S S 2021 Nanoconfining solution-processed organic semiconductors for emerging optoelectronics *Chem. Soc. Rev.* **50** 9375–90

[41] Wang J *et al* 2020 Gold nanoframeworks with mesopores for raman–photoacoustic imaging and photo-chemo tumor therapy in the second near-infrared biowindow *Adv. Funct. Mater.* **30** 1908825

[42] Wang G L, Zhu X Y, Dong Y M, Jiao H J, Wu X M and Li Z J 2013 The pH-dependent interaction of silver nanoparticles and hydrogen peroxide: A new platform for visual detection of iodide with ultra-sensitivity *Talanta* **107** 146–53

[43] He X N, Gao Y, Mahjouri-Samani M, Black P N, Allen J, Mitchell M, Xiong W, Zhou Y S, Jiang L and Lu Y F 2012 Surface-enhanced Raman spectroscopy using gold-coated horizontally aligned carbon nanotubes *Nanotechnology* **23** 205702

[44] Han Y, Lupitskyy R, Chou T-M, Stafford C M, Du H and Sukhishvili S 2011 Effect of oxidation on surface-enhanced raman scattering activity of silver nanoparticles: a quantitative correlation *Anal. Chem.* **83** 5873–80

[45] Le Ru E C, Blackie E, Meyer M and Etchegoint P G 2007 Surface enhanced raman scattering enhancement factors: A comprehensive study *J. Phys. Chem.* C **111** 13794–803

[46] Zhang Y, Hu Y, Li G and Zhang R 2019 A composite prepared from gold nanoparticles and a metal organic framework (type MOF-74) for determination of 4-nitrothiophenol by surface-enhanced Raman spectroscopy *Microchim. Acta* **186** 1–10

[47] Qiu L, Pang G A, Zheng G, Bauer D, Wieland K and Haisch C 2020 Kinetic and mechanistic investigation of the photocatalyzed surface reduction of 4-nitrothiophenol observed on a silver plasmonic film via surface-enhanced raman scattering *ACS Appl. Mater. Interfaces* **12** 21133–42

[48] Mahmoud M A, Garlyyev B and El-Sayed M A 2013 Determining the mechanism of solution metallic nanocatalysis with solid and hollow nanoparticles: Homogeneous or heterogeneous *J. Phys. Chem.* C **117** 21886–93

[49] Huang J, Zhu Y, Lin M, Wang Q, Zhao L, Yang Y, Yao K X and Han Y 2013 Site-specific growth of Au-Pd alloy horns on Au nanorods: A platform for highly sensitive monitoring of catalytic reactions by surface enhancement raman spectroscopy *J. Am. Chem. Soc.* **135** 8552–61

[50] Zheng G, Polavarapu L, Liz-Marzán L M, Pastoriza-Santos I and Pérez-Juste J 2015 Gold nanoparticle-loaded filter paper: A recyclable dip-catalyst for real-time reaction monitoring by surface enhanced Raman scattering *Chem. Commun.* **51** 4572–5

[51] Xie W, Herrmann C, Kömpe K, Haase M and Schlücker S 2011 Synthesis of bifunctional Au/Pt/Au core/shell nanoraspberries for *in situ* SERS monitoring of platinum-catalyzed reactions *J. Am. Chem. Soc.* **133** 19302–5